Magnetoresistance of an all-manganite spin valve: A thin antiferromagnetic insulator sandwiched between two ferromagnetic metallic electrodes

J. Salafranca, M. J. Calderón, and L. Brey
Instituto de Ciencia de Materiales de Madrid (CSIC), Cantoblanco, 28049 Madrid, Spain
(Received 18 October 2007; published 31 January 2008)

We study the magnetic and transport properties of an all-manganite spin valve consisting of a thin antiferromagnetic and insulating manganite sandwiched between two ferromagnetic and metallic manganite electrodes. When the ferromagnetic electrodes are in a parallel configuration, the double-exchange mechanism in the middle manganite slab is enhanced and the whole heterostructure becomes metallic. In the antiparallel alignment of the electrodes, the antiferromagnetic order in the middle layer is more robust and the resistance of the heterostructure is larger than in the parallel configuration. The strong dependence of the electronic structure of the middle manganite on the relative orientation of the magnetization in the leads turns out in a large tunneling magnetoresistance. We also find that the application of a magnetic field to the heterostructure in the parallel metallic configuration increases the electrical conductance, producing a large magnetoresistance. We discuss our conclusions in the context of recent experiments performed in manganite heterostructures.

DOI: 10.1103/PhysRevB.77.014441 PACS number(s): 75.47.Gk, 75.10.−b, 75.30.Kz, 75.50.Ee

Heterostructures of strongly correlated systems are currently in the spotlight due to the appearance of new electronic phases (electronic reconstruction) at their interfaces. A high mobility two-dimensional electron gas forms at the interface between a correlated Mott insulator and a band insulator.[1–3] At the interfaces between ferromagnetic (FM) metallic manganites and insulators, charge, orbital, and spin ordered phases[4,5] appear. Manganese perovskites are especially interesting because of their potential application in spintronics:[6] in the ferromagnetic phase, they are half-metals[7,8] and, therefore, very efficient spin injectors and detectors.[9–11] Furthermore, some manganites show an extremely large (colossal) magnetoresistance (CMR), and phase separation, fruit of the competition between very different phases ranging from metallic and FM to insulating and antiferromagnetic (AF).[12,13]

Manganites have the composition $R_{1-x}A_xMnO_3$, where R and A indicate trivalent and divalent ions, respectively. In these oxides, x coincides with the concentration of holes in the system. By changing the hole doping and/or the size of the ions of the manganites, different electronic and magnetic phases arise. For instance, $La_{1-x}Sr_xMnO_3$ (LSMO) is FM and metallic at the so-called optimal doping ($x \sim 1/3$) with a Curie temperature (T_C) above room temperature. $La_{2/3}Ca_{1/3}MnO_3$ (LCMO) shows a strong coupling between electrical and magnetic properties, being the FM phase metallic and the paramagnetic phase insulating. Manganites with smaller ions, as $Pr_{2/3}Ca_{1/3}MnO_3$ (PCMO), present charge, orbital, and spin order (CE type,[14] see Fig. 1) and are insulators in all range of temperatures. In general, FM metallic phases are promoted by the kinetic energy associated with the motion of the carriers in the system through the so-called double-exchange mechanism.[15] On the contrary, insulating phases appear in materials where localization effects, such as AF interaction between Mn core spins and Jahn-Teller coupling, are the most important energy scale.

Because manganites present a strong coupling between the electric and magnetic properties, these materials are ideal candidates for spintronics applications. The most popular existing spintronic devices are spin valves. A spin valve is a three layered device, with a first FM lead that is used as a spin polarizer, a nonferromagnetic spacer, and a second FM lead used as spin analyzer. These devices are based on the fact that the electrical resistance of a material connected to a spin polarized source and drain strongly depends on their relative orientation. The efficiency of a spin valve is given by tunneling magnetoresistance (TMR),[16] defined as the difference in resistance R between parallel (P) and antiparallel (AP) relative orientations of the magnetization in the FM metallic electrodes $[\mathrm{TMR}=(R_{AP}-R_P)/R_{AP}]$.

Manganite surfaces are known to behave differently from the bulk, the typical example being the striking suppression of the spin polarization of a free surface at temperatures much lower than the bulk ferromagnetic T_C.[17,18] This could have a very negative effect on the efficiency of spin valves because TMR depends very strongly on the properties of the electrode/barrier interface.[19] Indeed, early reports of TMR in manganite heterostructures showed a very strong decrease with increasing temperature.[20] The reduction of the spin polarization at the interface occurs because the lack of carriers at the interface attenuates the double-exchange FM coupling between the Mn ions.[5] Also, strain at the interfaces might lead to a depression of the magnetic properties of the manganite FM layer.[21] The optimization of structural matching and the use of nonpolar interfaces make possible to achieve spin polarization close to that of the bulk up to higher temperatures,[10,22,23] with the concomitant enhancement of TMR. Alternatively, the use of an insulating manganite as a spacer in the spin valve would provide a very good match to the lattice structure of the electrodes and a smoother variation of the carrier density.

In manganite heterostructures, the interfaces play a key role in determining the electric and magnetic properties. In Ref. 24, Li *et al.* tried to obtain high values of magnetoresistance (MR) by growing multilayers of LCMO and PCMO. For very thin layers of PCMO ($\leqslant 20$ Å) separated by thicker layers of LCMO, transport properties present an interesting behavior as a function of temperature. As temperature is low-

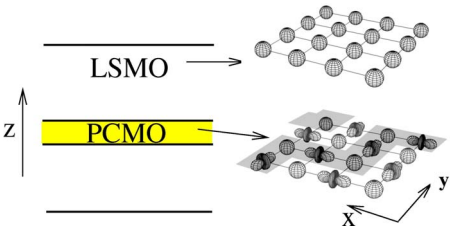

FIG. 1. (Color online) Schematic view of the heterostructure under consideration. LSMO stands for $La_{2/3}Sr_{1/3}MnO_3$ and PCMO for $Pr_{2/3}Ca_{1/3}MnO_3$. At this doping ($x=1/3$), bulk LSMO is FM and metallic, and bulk PCMO is CE-type AF, with FM zig zag chains in the xy plane antiferromagnetically coupled to neighboring chains, orbital and charge ordered and insulating.

ered, two transitions are found. First, a paramagnetic-ferromagnetic transition takes place, it is accompanied by a change in the slope sign of the resistivity as a function of temperature. This behavior is also observed in pure LCMO, suggesting that LCMO layers order FM at this temperature. In a second transition, magnetization increases and resistivity suddenly drops (~50% decay in 1 K). The authors attribute this drop to the onset of ferromagnetism in all the system. Similar results were obtained in Refs. 25 and 26. Notice that FM order can be induced in bulk PCMO, but a magnetic field of 2 T is needed.[12] In LSMO/LCMO based heterostructures, T_C and the range where large MR exists increase with respect to LCMO.[27–29] Finally, Niebieskikwiat *et al.*[30] studied, by means of polarized neutron reflectometry, the magnetization profile along the growth direction in a LSMO/PCMO multilayer. They found that a FM moment is induced in the PCMO layers.

In this work, we study a spin valve where the barrier is an AF insulating manganite and analyze the charge distribution, magnetic ordering, and the interplay of the different orders in the different layers. In particular, calculations are performed in the trilayer $La_{2/3}Sr_{1/3}MnO_3/Pr_{2/3}Ca_{1/3}MnO_3/La_{2/3}Sr_{1/3}MnO_3$ illustrated in Fig. 1 (multilayers with the same composition were experimentally studied in Ref. 30). Our main results are (i) a FM moment is induced in the PCMO layer in accordance with Ref. 30, (ii) the ground state configuration in the PCMO layer depends on the relative orientation of the magnetization in the LSMO layers and, as a consequence, the system shows a large TMR (see Fig. 3), and (iii) in the P configuration, the application of an external magnetic field affects the PCMO layer magnetic ordering giving rise to negative MR (see Fig. 4). In general, we find that the itinerant carriers in the leads try to minimize their kinetic energy penetrating into the insulating spacer. This enhances the FM double-exchange mechanism in the first layers of the manganite barrier and produces an effectively thinner insulating barrier.

We address these issues by finding the minimal energy spin, charge, and orbital configuration in a very thin PCMO spacer [two (PCMO-2) to three (PCMO-3) lattice parameters a wide] between two wider and perfectly ferromagnetic LSMO layers. The tight-binding Hamiltonian has the following terms:[5]

$$H = -\sum_{i,j,\gamma,\gamma'} f_{i,j} t^{u}_{\gamma,\gamma'} C^{\dagger}_{i,\gamma} C_{j,\gamma'} + \sum_{i,j} J^{ij}_{AF} \mathbf{S}_i \mathbf{S}_j + U' \sum_{i} \sum_{\gamma \neq \gamma'} n_{i\gamma} n_{i\gamma'} + H_{\text{Coulomb}}, \quad (1)$$

where $C^{\dagger}_{i,\gamma}$ creates an electron on the Mn i site, in the e_g orbital γ ($\gamma=1,2$, with $1=|x^2-y^2\rangle$ and $2=|3z^2-r^2\rangle$). Here, $\langle n_i\rangle=\Sigma_\gamma\langle C^{\dagger}_{i,\gamma}C_{i,\gamma}\rangle$ is the occupation number on the Mn i site. The hopping amplitude depends on the Mn core spin orientation given by the angles θ and ψ via $f_{i,j} = \cos(\theta_i/2)\cos(\theta_j/2) + \exp[i(\psi_i-\psi_j)]\sin(\theta_i/2)\sin(\theta_j/2)$ (double-exchange mechanism) and on the orbitals involved $t^{x(y)}_{1,1} = \pm\sqrt{3}t^{x(y)}_{1,2} = \pm\sqrt{3}t^{x(y)}_{2,1} = 3t^{x(y)}_{2,2} = 3/4t^{z}_{2,2} = t$, where the super-indices x, y, and z refer to the directions in the lattice. All the parameters are given in units of t which is estimated to be ~0.2–0.5 eV. J_{AF} is an effective antiferromagnetic coupling between first neighbor Mn core spins, which is different in the LSMO and PCMO layers (see below). U' is a repulsive interaction between electrons on a site lying on different orbitals, and H_{Coulomb} is the long range Coulomb interaction between all the charges in the system, treated in the mean-field approximation,

$$H_{\text{Coulomb}} = \frac{e^2}{\epsilon}\sum_{i\neq j}\left(\frac{1}{2}\frac{\langle n_i\rangle\langle n_j\rangle}{|\mathbf{R}_i-\mathbf{R}_j|} + \frac{1}{2}\frac{Z_iZ_j}{|\mathbf{R}^A_i-\mathbf{R}^A_j|} - \frac{Z_i\langle n_j\rangle}{|\mathbf{R}^A_i-\mathbf{R}_j|}\right), \quad (2)$$

with $\mathbf{R}_i$ the position of the Mn ions, eZ_i the charge of the A cation located at $\mathbf{R}^A_i$, and ϵ the dielectric constant of the material. The strength of the Coulomb interaction is given by the dimensionless parameter $\alpha=e^2/a\epsilon t$.[4]

The electron-lattice interaction has not been explicitly included in the Hamiltonian (1). However, the effect of this coupling on the ground state energies can be described using an effective J_{AF}.[31] In particular, the ground state of Hamiltonian (1) for a bulk system with $J_{AF}\gtrsim 0.2t$ is the CE-type AF ordering associated with the lattice distortions that produce the charge and orbital ordering, as illustrated in Fig. 1. The values for J_{AF} that effectively include the electron-lattice coupling are therefore larger than the ones inferred from the magnetic ordering only (J^S_{AF} from superexchange between the t_{2g} electrons is ~1–10 meV).[12] For each of the layers, we choose appropriate values of J_{AF} that describe well the bulk phases: small values of J_{AF} for the LSMO FM configuration (for simplicity, we consider $J_{\text{LSMO}}=0$) and $0.15t < J_{\text{PCMO}} < 0.3t$ for the PCMO CE-type ordering (PCMO shows CE-type ordering in a wide range of dopings).[32] Reasonable values for the other two parameters are $U'=2t$ and $\alpha=2$.[5] The results presented below are qualitatively insensitive to moderate changes of these two parameters. The Hamiltonian is solved in heterostructures consisting of a thin PCMO layer and two wide LSMO FM layers (wide enough to reproduce bulk behavior): for a given configuration of the Mn core spins, the Hamiltonian is diagonalized numerically iteratively until self-consistency in the Hartree potential and the charges is reached.

In Fig. 2, we show the total energy versus J_{PCMO} for a pure FM, CE, and an intermediate *canted* configuration of

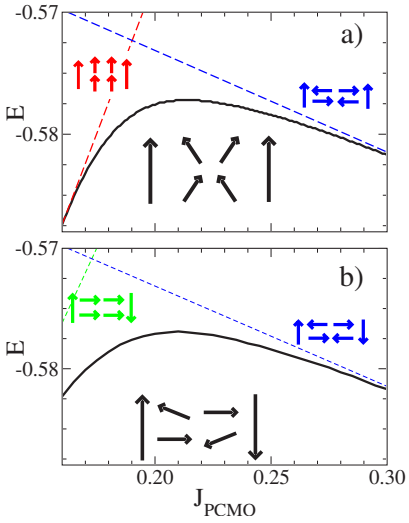

FIG. 2. (Color online) Energy versus J_{PCMO} for (a) parallel and (b) antiparallel configurations of the LSMO layers, with PCMO thickness of two lattice parameters, PCMO-2. The dashed lines are the energy for the pure FM and pure CE configurations in the intermediate PCMO layer. The actual ground state (solid line) corresponds to canted intermediate configurations (illustrated in the insets). The big arrows represent the magnetization orientation in the FM layers and the small ones represent the order considered in the PCMO-2 layer. In the CE and canted phases, each arrow in the PCMO layer represents a FM zigzag chain (see Fig. 1).

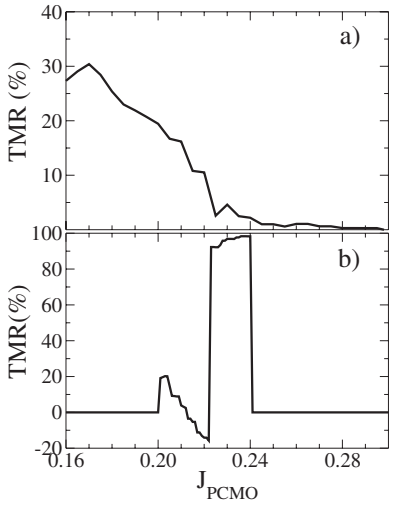

FIG. 3. Tunneling magnetoresistance versus J_{PCMO} calculated for PCMO layer thicknesses of (a) two and (b) three lattice parameters. For large values of J_{PCMO}, the TMR is very small because the PCMO spacer is AF and insulating for both P and AP configurations. For $J_{PCMO} < 0.24t$, (a) and (b) show different qualitative behaviors (see text for discussion). The maximum sensitivity to magnetization is reached in PCMO-3 for $0.22t < J_{PCMO} < 0.24t$, where the system is metallic in the P configuration while insulating in the AP configuration.

the PCMO-2 layer for P and AP configurations of the electrodes. All the other magnetic orderings considered were higher in energy in this range of parameters. For $0.17t < J_{PCMO} < 0.3t$, the magnetic ground state configuration in the spacer is always canted with the canting angle depending on the value of J_{PCMO} and on the relative orientation of the magnetization in the LSMO layers. In the P configuration [Fig. 2(a)], PCMO tends to order more FM and collinearly with the electrodes, while for the AP case [Fig. 2(b)], the PCMO configuration corresponds to smaller magnetization and the spins lie perpendicular to the electrodes magnetization. The results for PCMO-3 (not shown) are qualitatively similar.

For PCMO-2 and J_{PCMO} relatively small ($\lesssim 0.24t$), the magnetic order at the barrier is canted and the charge and orbital order is mostly suppressed due to charge transfer between the layers. FM correlations and, due to double exchange, conductance are larger in the P configuration than in the AP configuration. Therefore, this geometry could be used as a magnetic sensor. The conductance has been calculated numerically via the Kubo formula[33,34] for a trilayer with semi-infinite FM LSMO leads. The results for a PCMO-2 spacer are plotted in Fig. 3(a) where a finite TMR for $J_{PCMO} \lesssim 0.24t$ is shown. The superstructure in the curve is due to numerical inaccuracies except for the peak at $J_{PCMO} \sim 0.17t$, which is quite robust (the TMR increases monotonically in the range $0.1t < J_{PCMO} \lesssim 0.17t$). This peak appears because, below $\sim 0.17t$, the P ground state configuration is almost FM [Fig. 2(a)] while the AP configuration is already canted [Fig. 2(b)] and, as a consequence, R_{AP} increases faster with J_{PCMO} than R_P.

For PCMO-3, there is a range of parameters, $0.22t \lesssim J_{PCMO} \lesssim 0.24t$, for which the TMR is close to its maximum possible value of 100%. This relatively narrow range of J_{PCMO} is expected to have physical relevance for PCMO at some doping of $0.3 \lesssim x \lesssim 0.7$.[32] In this range, the P configuration is metallic as it has a relatively large FM component in the three Mn planes that constitute the barrier, while the AP configuration is insulating and corresponds to perfect CE in the middle atomic plane and canted FM in the outer planes. For smaller values of J_{PCMO} ($\lesssim 0.2t$), for both the P and AP configurations, the middle plane is a perfect CE, while the outer planes are essentially FM and parallel to the nearest electrode; this leads to $R_P = R_{AP}$ and, hence, TMR=0. The negative TMR at $J_{PCMO} \sim 0.22t$ is produced by the different dependences of the canting angle on J_{PCMO} for P and AP configurations. A different behavior of the TMR in PCMO-2 and PCMO-3 is due to the limited charge transfer in the middle Mn plane of the wider barrier. For large J_{PCMO} ($>0.24t$) [see Figs. 3(a) and 3(b)], the AF ordering in the barrier is preserved and the system does not show TMR at all: both R_P and R_{AP} tend to ∞. A systematic analysis for wider barriers is out of our computational capabilities. The calculations indicate that the penetration of the wave functions of the FM leads into the insulating barrier is always limited to the first two or three layers, and therefore these results suggest that significant values of TMR are either absent or appear in a narrow range of parameters for barriers thicker than three atomic layers.

We have also calculated the MR in the P configuration that results of applying an external magnetic field parallel to the magnetization in the electrodes H_x. This adds a Zeeman term to the Hamiltonian: $g\mu_B H_x \Sigma_i S_{ix}$. The results are shown

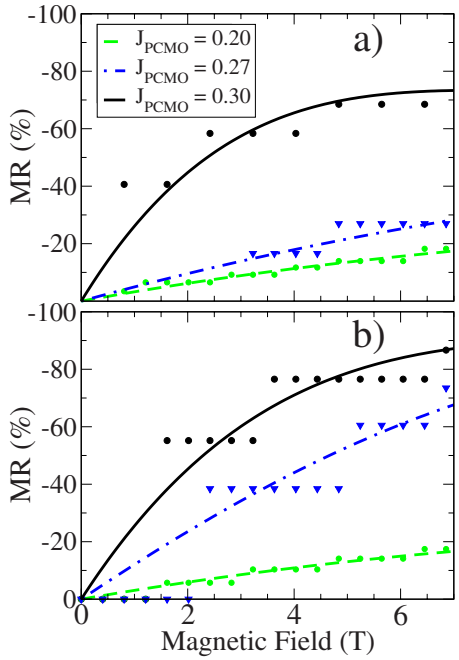

FIG. 4. (Color online) Magnetoresistance in the parallel configuration upon application of a small magnetic field in the x direction for three different values of J_{PCMO}: (a) PCMO-2 and (b) PCMO-3. Here, $t=0.25$ eV is used for the estimation of the magnetic field H. The lines are fits to the dots.

for PCMO-2 and PCMO-3 in Fig. 4. We define MR $=[R(H)-R(0)]/R(0)\times 100\%$ so its maximum possible absolute value is MR$=100\%$. The dots represent the numerical values and the steps are an artifice of the calculation that considers a discrete set of values of the canting angle. The lines are a fit to the data. When a magnetic field H is applied, the system is effectively moving toward smaller values of J_{PCMO} (see Fig. 2) and therefore toward less resistive configurations, hence the negative MR. This MR is produced by the alignment of the barrier spins with the applied field and is smaller than the CMR measured in bulk PCMO[35] which is probably related to inhomogeneities and phase separation. The real advantage of this heterostructure as a device is that its resistivity can be orders of magnitude smaller than the bulk PCMO's (mainly because there is no gap at the Fermi energy for the thin spacers in the P configuration). As a guideline, the resistivity of bulk LSMO at low T is $\sim 10^{-4}$ Ω cm,[36] much smaller than that of bulk PCMO $\gtrsim 10^5$ Ω cm ($\sim 10^{-3}$ Ω cm at 7 T).[37] These results agree with the experimental work presented in Ref. 24. For LCMO (100 Å)/PCMO (15 Å) multilayers, they find that metallicity is induced in PCMO at low temperatures. The behavior of resistivity versus temperature also agrees with the results in Fig. 2. As T is raised, spin disorder reduces the effective hopping, and the relative strength of the superexchange interaction J_{PCMO} increases. This explains the experimental observation that ferromagnetic correlations in PCMO are lost with increasing temperature.[24,25]

It is well known that strain (produced by lattice mismatch between the substrate and the thin films) can affect the orbital ordering.[38] In heterostructures with an $SrTiO_3$ substrate,[30] the in-plane lattice parameter is 3.90 Å for all layers while the out-of-plane lattice parameters are 3.85 Å (LSMO) and 3.76 Å (PCMO), slightly smaller (less than a 2% in any case) than the bulk values. Our calculations are done in a cubic lattice, but the variations in unit cell dimensions in actual heterostructures[30] are not expected to produce a dramatic change in the orbital ordering.[38] In any case, it would emphasize the tendency to CE ordering in the PCMO barrier that can be included in our model simply by increasing the value of J_{PCMO}. Strain can also produce phase separation[21] and colossal magnetoresistance.[39] The inclusion of phase separation in our model would lead to an increase of both TMR (Fig. 3) and MR (Fig. 4) with respect to the calculated values. Our calculations are done at $T=0$. Qualitatively, the MR and TMR in these heterostructures are expected to survive up to the critical temperatures of the FM ordering in the electrodes and the AF ordering in the spacer ($\gtrsim$200 K).[32]

In conclusion, we study an all-manganite trilayer. It is composed of two ferromagnetic metallic manganite electrodes ($La_{2/3}Sr_{1/3}MnO_3$) and a thin AF manganite barrier ($Pr_{2/3}Ca_{1/3}MnO_3$). Both materials have, *a priori*, suitable properties for an efficient spin valve device. LSMO is half metallic, and it has relatively low resistivity. PCMO grows in the same crystal structure as LSMO and with a very similar lattice parameter. We find that the spin valve presents high values of TMR. The ground state configuration in the PCMO layer depends on the relative orientation of the magnetization in the FM electrodes. For a relevant range of parameters, the electronic state of the PCMO slab in the parallel configuration is metallic, whereas it is insulating in the antiparallel arrangement. Therefore, it might be possible to reversibly switch the system between a metallic and insulating state. We also find that, due to the coupling of the electrical and magnetic properties, the resistance of the heterostructure depends on an applied field, presenting large negative magnetoresistance. These effects are manifestations of the enhancement of double-exchange effects in the AF slab due to the presence of the neighbors FM slabs. This mechanism explains some experimental observations in manganite multilayers: the onset of a metallic state,[24,25] the reduction of resistivity, and the increase of magnetoresistance.[26–29]

We thank J. A. Vergés for fruitful discussions. This work is supported by MAT2006-03741 (MEC, Spain). J.S. also acknowledges the FPU program (MEC, Spain) and M.J.C. the Ramón y Cajal program (MEC, Spain).

[1] S. Okamoto and A. Millis, Nature (London) **428**, 630 (2004).
[2] M. Huijben, G. Rijnders, D. H. A. Blank, S. Bals, S. V. Aert, J. Verbeeck, G. V. Tendeloo, A. Brinkman, and H. Hilgenkamp, Nat. Mater. **5**, 556 (2006).
[3] S. S. Kancharla and E. Dagotto, Phys. Rev. B **74**, 195427 (2006).
[4] C. Lin, S. Okamoto, and A. J. Millis, Phys. Rev. B **73**, 041104(R) (2006).
[5] L. Brey, Phys. Rev. B **75**, 104423 (2007).
[6] I. Zutic, J. Fabian, and S. Das Sarma, Rev. Mod. Phys. **76**, 323 (2004).
[7] W. E. Pickett and D. J. Singh, Phys. Rev. B **53**, 1146 (1996).
[8] J.-H. Park, E. Vescovo, H.-J. Kim, C. Kwon, R. Ramesh, and T. Venkatesan, Nature (London) **392**, 794 (1998).
[9] M. Bowen, M. Bibes, A. Barthelemy, J.-P. Contour, A. Anane, Y. Lemaitre, and A. Fert, Appl. Phys. Lett. **82**, 233 (2003).
[10] H. Yamada, Y. Ogawa, Y. Ishii, H. Sato, M. Kawasaki, H. Akoh, and Y. Tokura, Science **305**, 646 (2004).
[11] M. Bibes and A. Barthélémy, IEEE Trans. Electron Devices **54**, 1003 (2007).
[12] E. Dagotto, *Nanoscale Phase Separation and Colossal Magnetoresistance* (Springer-Verlag, Berlin, 2003).
[13] C. Israel, M. J. Calderón, and N. D. Mathur, Mater. Today **10**, 24 (2007).
[14] J. B. Goodenough, Phys. Rev. **100**, 564 (1955), see Fig. 4.
[15] C. Zener, Phys. Rev. **82**, 403 (1951).
[16] M. Jullière, Phys. Lett. **54A**, 225 (1975).
[17] J.-H. Park, E. Vescovo, H.-J. Kim, C. Kwon, R. Ramesh, and T. Venkatesan, Phys. Rev. Lett. **81**, 1953 (1998).
[18] M. J. Calderón, L. Brey, and F. Guinea, Phys. Rev. B **60**, 6698 (1999).
[19] P. LeClair, H. J. M. Swagten, J. T. Kohlhepp, R. J. M. van de Veerdonk, and W. J. M. de Jonge, Phys. Rev. Lett. **84**, 2933 (2000).
[20] Y. Lu, X. W. Li, G. Q. Gong, G. Xiao, A. Gupta, P. Lecoeur, J. Z. Sun, Y. Y. Wang, and V. P. Dravid, Phys. Rev. B **54**, R8357 (1996).
[21] I. Infante, S. Estradé, F. Sánchez, J. Arbiol, F. Peiró, V. Laukhin, J. P. Espinós, M. Wojcik, E. Jedryka, and J. Fontcuberta, Phys. Rev. B **76**, 224415 (2007).
[22] V. Garcia, M. Bibes, A. Barthelemy, M. Bowen, E. Jacquet, J.-P. Contour, and A. Fert, Phys. Rev. B **69**, 052403 (2004).
[23] Y. Ishii, H. Yamada, H. Sato, H. Akoh, Y. Ogawa, M. Kawasaki, and Y. Tokura, Appl. Phys. Lett. **89**, 042509 (2006).
[24] H. Li, J. R. Sun, and H. K. Wong, Appl. Phys. Lett. **80**, 628 (2002).
[25] A. Venimadhav, M. Hegde, R. Rawat, I. Das, and M. El Marssi, J. Alloys Compd. **326**, 270 (2001).
[26] G. Lian, Z. Wang, J. Gao, J. Kang, M. Li, and G. Xiong, J. Phys. D **32**, 90 (1999).
[27] L. Alldredge and Y. Suzuki, Appl. Phys. Lett. **85**, 437 (2004).
[28] M. Jain, P. Shukla, Y. Li, M. Hundley, H. Wang, S. Foltyn, A. Burrell, T. Mccleskey, and Q. Jia, Adv. Mater. (Weinheim, Ger.) **18**, 2695 (2006).
[29] S. Mukhopadhyay and I. Das, Appl. Phys. Lett. **88**, 032506 (2006).
[30] D. Niebieskikwiat, M. B. Salomon, L. E. Hueso, N. D. Mathur, and J. A. Borchers, Phys. Rev. Lett. **99**, 247207 (2007).
[31] J. van den Brink, G. Khaliullin, and D. Khomskii, Phys. Rev. Lett. **83**, 5118 (1999).
[32] M. v. Zimmermann, C. S. Nelson, J. P. Hill, D. Gibbs, M. Blume, D. Casa, B. Keimer, Y. Murakami, C.-C. Kao, C. Venkataraman, T. Gog, Y. Tomioka, and Y. Tokura, Phys. Rev. B **64**, 195133 (2001).
[33] J. Vergés, Comput. Phys. Commun. **118**, 71 (1999).
[34] M. J. Calderón, J. A. Vergés, and L. Brey, Phys. Rev. B **59**, 4170 (1999).
[35] A. Anane, J.-P. Renard, L. Reversat, C. Dupas, P. Veillet, M. Viret, L. Pinsard, and A. Revcolevschi, Phys. Rev. B **59**, 77 (1999).
[36] A. Urushibara, Y. Moritomo, T. Arima, A. Asamitsu, G. Kido, and Y. Tokura, Phys. Rev. B **51**, 14103 (1995).
[37] H. Yoshizawa, H. Kawano, Y. Tomioka, and Y. Tokura, J. Phys. Soc. Jpn. **65**, 1043 (1996).
[38] Y. Tokura and N. Nagaosa, Science **288**, 462 (2000).
[39] K. Ahn, T. Lookman, and A. Bishop, Nature (London) **428**, 401 (2004).